SFN #347 13-18

藤井　通子

The Effects of Starspots on Spectroscopic Mass Estimates of Low-mass Young Stars

C. Flores [1], M. S. Connelley [1], B. Reipurth [1], and G. Duchêne [2,3]

Magnetic fields and mass accretion processes create dark and bright spots on the surface of young stars. These spots manifest as surface thermal inhomogeneities, which alter the global temperature measured on the stars. To understand the effects and implications of these starspots, we conducted a large iSHELL high-resolution infrared spectroscopic survey of T Tauri stars in Taurus-Auriga and Ophiuchus star-forming regions. From the K band spectra, we measured stellar temperatures and magnetic field strengths using a magnetic radiative transfer code. We compared our infrared-derived parameters against literature optical temperatures and found a) a systematic temperature difference between optical and infrared observations, and b) a positive correlation between the magnetic field strengths and the temperature differences. The discrepant temperature measurements imply significant differences in the inferred stellar masses from stellar evolutionary models. To discern which temperature better predicts the mass of the star, we compared our model-derived masses against dynamical masses measured from ALMA and PdBI for a sub-sample of our sources. From this comparison we conclude that, in the range of stellar masses from 0.3 to 1.3 $M_\odot$, neither infrared nor optical temperatures perfectly reproduce the stellar dynamical masses. But, on average, infrared temperatures produce more precise and accurate stellar masses than optical ones.

Binary Formation in the Orion Nebula Cluster: Exploring the Sub-stellar Limit

Matthew De Furio,[1] Michael R. Meyer,[1] Megan Reiter,[2] John Monnier,[1] Adam Kraus,[3] and Trent Dupuy[4]

We present results constraining the multiplicity of the very low mass stars and sub-stellar objects in the Orion Nebula Cluster (ONC). Our sample covers primary masses 0.012-0.1$M_\odot$ using archival Hubble Space Telescope data obtained with the Advanced Camera for Surveys using multiple filters. Studying the binary populations of clusters provides valuable constraints of how the birth environment affects binary formation and evolution. Prior surveys have shown that the binary populations of high-mass, high-density star clusters like the ONC may substantially differ from those in low-mass associations. Very low mass stellar and sub-stellar binaries at wide separations, >20AU, are statistically rare in the Galactic field and have been identified in stellar associations like Taurus-Auriga and Ophiuchus. They also may be susceptible to dynamical interactions, and their formation may be suppressed by feedback from on-going star formation. We implement a double point-spread function (PSF) fitting algorithm using empirical, position dependent PSF models to search for binary companions at projected separations > 10 AU (0.025"). With this technique, we identify 7 very low mass binaries, 5 of which are new detections, resulting in a binary frequency of $12^{+6}_{-3.2}$% over mass ratios of 0.5 - 1.0 and projected separations of 20 - 200 AU. We find an excess of very low mass binaries in the ONC compared to the Galactic field, with a probability of 10^{-6} that the populations are statistically consistent. The sub-stellar population of the ONC may require further dynamical processing of the lowest binding energy binaries to resemble the field population.

- ONCの低質量星で20-200au離れた連星を探した
- Double-PSF fitting
- ONCでlow-mass binaryがフィールドより多い
- このあと力学的に壊される？？

ALMA chemical survey of disk-outflow sources in Taurus (ALMA-DOT) VI: Accretion shocks in the disk of DG Tau and HL Tau

A. Garufi[1], L. Podio[1], C. Codella[1,2], D. Segura-Cox[3], M. Vander Donckt[4], S. Mercimek[1,5], F. Bacciotti[1], D. Fedele[1], M. Kasper[4], J. E. Pineda[3], E. Humphreys[6,4], and L. Testi[4,1]

Planet-forming disks are not isolated systems. Their interaction with the surrounding medium affects their mass budget and chemical content. In the context of the ALMA-DOT program, we obtained high-resolution maps of assorted lines from six disks that are still partly embedded in their natal envelope. In this work, we examine the SO and SO_2 emission that is detected from four sources: DG Tau, HL Tau, IRAS 04302+2247, and T Tau. The comparison with CO, HCO^+, and CS maps reveals that the SO and SO_2 emission originates at the intersection between extended streamers and the planet-forming disk. Two targets, DG Tau and HL Tau, offer clear cases of inflowing material inducing an accretion shock on the disk material. The measured rotational temperatures and radial velocities are consistent with this view. In contrast to younger Class 0 sources, these shocks are confined to the specific disk region impacted by the streamer. In HL Tau, the known accreting streamer induces a shock in the disk outskirts, and the released SO and SO_2 molecules spiral toward the star in a few hundred years. These results suggest that shocks induced by late accreting material may be common in the disks of young star-forming regions with possible consequences for the chemical composition and mass content of the disk. They also highlight the importance of SO and SO_2 line observations in probing accretion shocks from a larger sample.

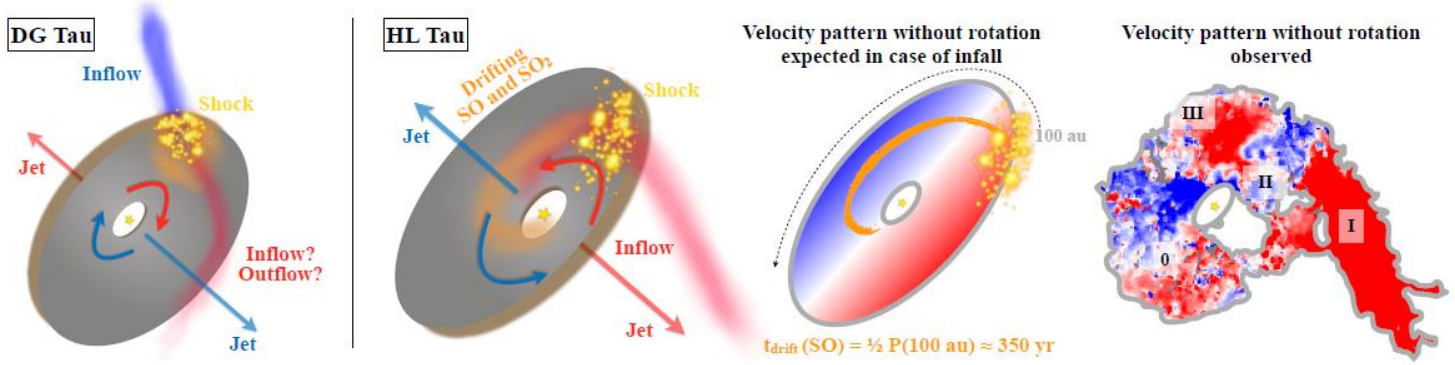

Fig. 7. Illustrative sketch of the environment of DG Tau and HL Tau. The third panel shows the velocity pattern expected in case of uniform infall after rotation subtraction. The fourth panel shows the observed HCO^+ velocity pattern after rotation subtraction (see Fig. 6).

A SPHERE survey of self-shadowed planet-forming disks

A. Garufi[1], C. Dominik[2], C. Ginski[2], M. Benisty[3,4], R.G. van Holstein[5], Th. Henning[6], N. Pawellek[7], C. Pinte[4], H. Avenhaus[8], S. Facchini[9,10], R. Galicher[11], R. Gratton[12], F. Ménard[4], G. Muro-Arena[2], J. Milli[4], T. Stolker[13], A. Vigan[14], M. Villenave[15,4], T. Moulin[4], A. Origne[14], F. Rigal[2], J.-F. Sauvage[16,14], and L. Weber[17]

To date, nearly two hundred planet-forming disks have been imaged with high resolution. Our propensity to study bright and extended objects is however biasing our view of the disk demography. In this work, we contribute to alleviate this bias by analyzing fifteen disks targeted with VLT/SPHERE that look faint in scattered light. Sources were selected based on a low far-IR excess from the spectral energy distribution. The comparison with the ALMA images available for a few sources shows that the scattered light surveyed by these datasets is only detected from a small portion of the disk extent. The mild anti-correlation between the disk brightness and the near-IR excess demonstrates that these disks are self-shadowed: the inner disk rim intercepts much starlight and leaves the outer disk in penumbra. Based on the uniform distribution of the disk brightness in scattered light across all spectral types, self-shadowing would act similarly for inner rims at a different distance from the star. We discuss how the illumination pattern of the outer disk may evolve with time. Some objects in the sample are proposed to be at an intermediate stage toward bright disks from the literature with either no shadow or with sign of azimuthally confined shadows.

- できるだけ無バイアスのサンプルを集めてみた

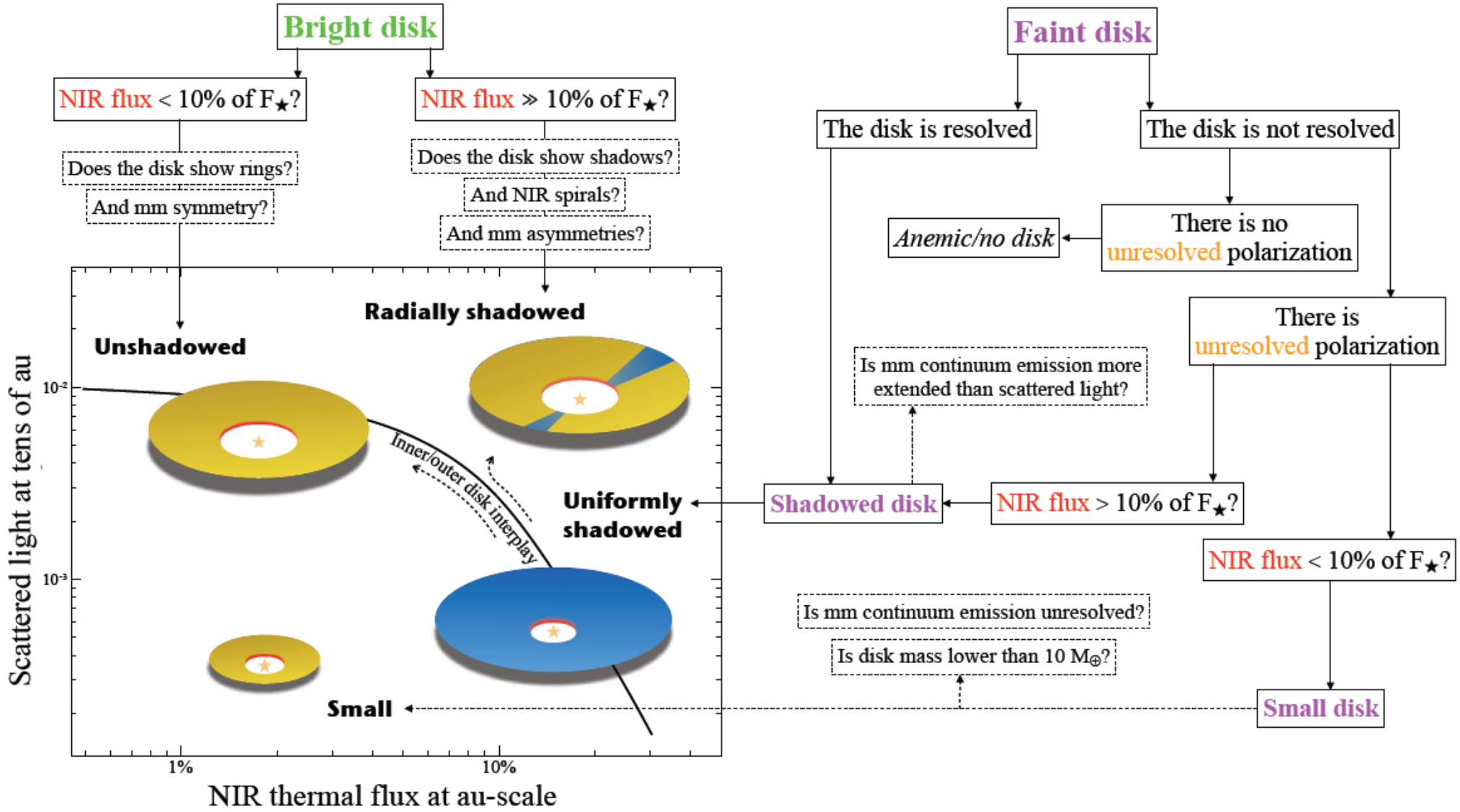
Bright disk
NIR flux < 10% of F★?
NIR flux ≫ 10% of F★?
Does the disk show rings?
And mm symmetry?
Does the disk show shadows?
And NIR spirals?
And mm asymmetries?
Faint disk
The disk is resolved
The disk is not resolved
Anemic/no disk
There is no unresolved polarization
There is unresolved polarization
Is mm continuum emission more extended than scattered light?
Shadowed disk
NIR flux > 10% of F★?
NIR flux < 10% of F★?
Is mm continuum emission unresolved?
Is disk mass lower than 10 M⊕?
Small disk
Unshadowed
Radially shadowed
Uniformly shadowed
Small
Inner/outer disk interplay
Scattered light at tens of au
10⁻²
10⁻³
1%
10%
NIR thermal flux at au-scale

Bottling the Champagne: Dynamics and Radiation Trapping of Wind-Driven Bubbles around Massive Stars

Sam Geen[1]★, Alex de Koter[1,2]

In this paper we make predictions for the behaviour of wind bubbles around young massive stars using analytic theory. We do this in order to determine why there is a discrepancy between theoretical models that predict that winds should play a secondary role to photoionisation in the dynamics of HII regions, and observations of young HII regions that seem to suggest a driving role for winds. In particular, regions such as M42 in Orion have neutral hydrogen shells, suggesting that the ionising radiation is trapped closer to the star. We first derive formulae for wind bubble evolution in non-uniform density fields, focusing on singular isothermal sphere density fields with a power law index of -2. We find that a classical "Weaver"-like expansion velocity becomes constant in such a density distribution. We then calculate the structure of the photoionised shell around such wind bubbles, and determine at what point the mass in the shell cannot absorb all of the ionising photons emitted by the star, causing an "overflow" of ionising radiation. We also estimate perturbations from cooling, gravity, magnetic fields and instabilities, all of which we argue are secondary effects for the conditions studied here. Our wind-driven model provides a consistent explanation for the behaviour of M42 to within the errors given by observational studies. We find that in relatively denser molecular cloud environments around single young stellar sources, champagne flows are unlikely until the wind shell breaks up due to turbulence or clumping in the cloud.

- M42 (Orion Nebula) のバブルの解析的なモデル計算
- 一様ではなく、isothermal sphere density fieldを仮定
- Wind-drivenモデルでバブルの形成は説明できる（cooling, gravity magnetic fieldは secondary effect）
- Geen+(2021)という星団形成シミュレーションの論文がある

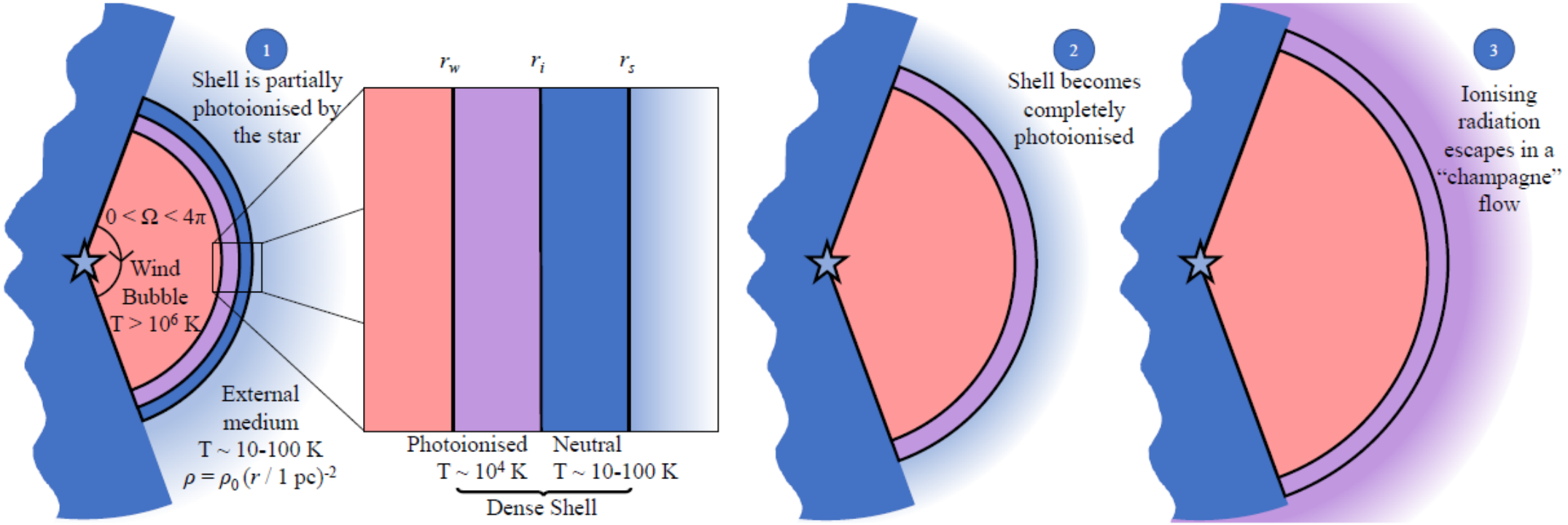

Figure 1. Diagram showing a schematic of the model used in this paper. 1) A hot ($> 10^6$ K) wind bubble (pink) expands from a stellar source at $r = 0$ into a conic section subtended by a solid angle Ω out to radius r_w. If $\Omega < 4\pi$, a wall of dense gas blocks its expansion in all other directions (blue, left part of the diagram). For the most part we ignore the "'free-streaming" phase described in Weaver et al. (1977) since it does not affect our result. The wind bubble expands into a neutral external density field with a power law distribution ($\rho = \rho_0 (r/1\mathrm{pc})^{-2}$, light blue gradient) and temperature $\sim 10 - 100$ K. A dense shell containing neutral hydrogen forms between r_i and r_s from the material swept up by the wind. The inner part of the shell (mauve) is photoionised by radiation from the star to $\sim 10^4$ K between r_w and r_i, while the outer part (blue) between r_i and r_s remains neutral at a similar temperature to the external medium. 2) As the wind bubble expands, more of the shell becomes photoionised until a point where the whole shell is photoionised. 3) The ionising radiation overflows the shell and creates a rapidly-expanding "champagne" flow into the external medium. In this paper we argue that the transition to phase 3 is unlikely in dense molecular cloud conditions until the wind shell is disrupted by some other effect, such as encountering another wind bubble or being broken up by asphericities in the cloud.

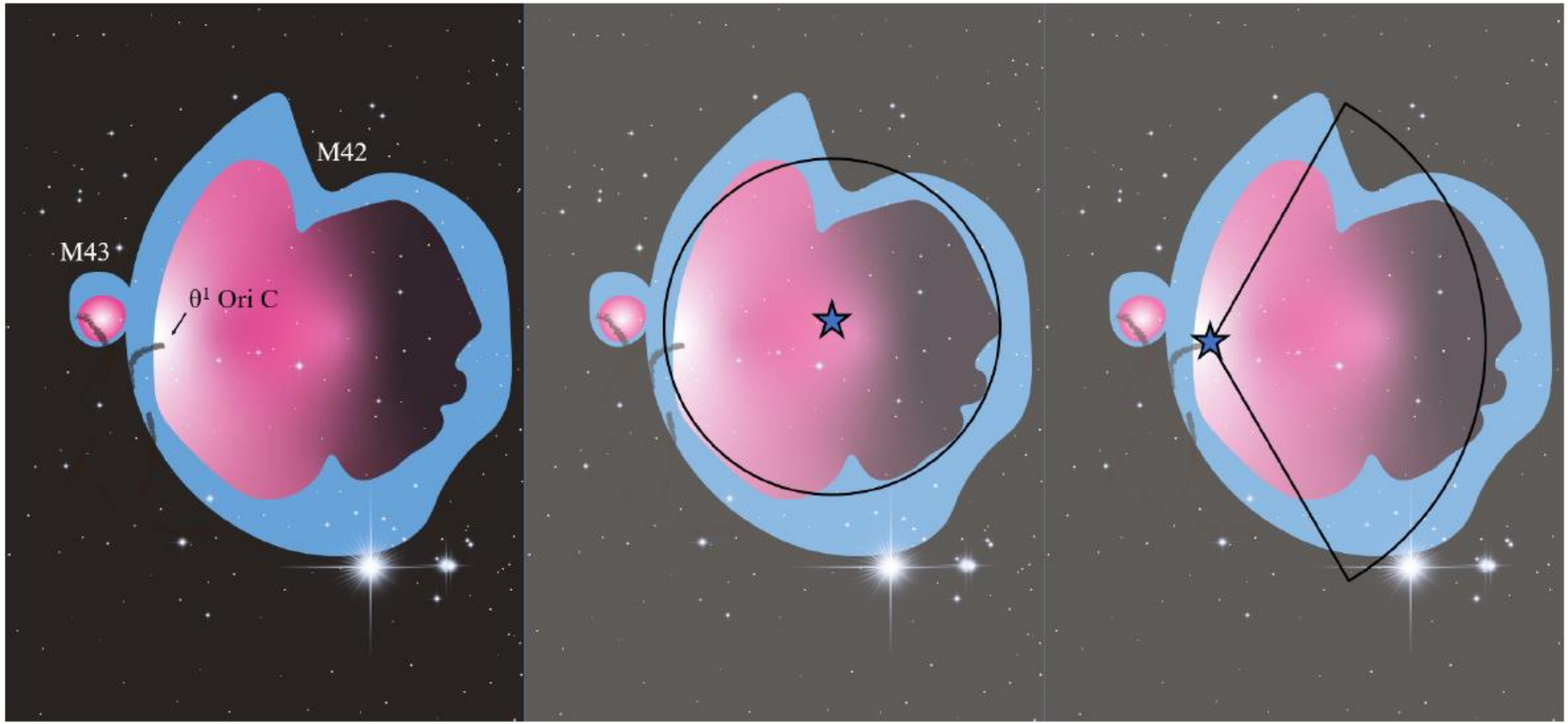

Figure 8. Schematic showing the model used to describe the Orion Nebula (M42). The image on the left shows the location of the principal components of the nebula, including the source of the feedback, star θ^1 Ori C in the Trapezium cluster, at the left edge of the nebula. The nearby nebula M43 is not treated in this work but is included for visual reference. The first model, a sphere centred on the nebula but not the star, is shown in the centre panel. The second model, a cone with its point located on the star with flows moving in a radial direction rightwards in a solid angle of π, is shown in the right panel. We discuss both models in Section 5.5.

1 We consider this distribution over an open angle Ω, with a maximum value of 4π if the density distribution extends across all lines of sight. Smaller values can be found if much denser gas constrains the bubble along certain lines of sight. The mass enclosed in radius r in the initial conditions is thus

$$M(<r) = \int_0^r \Omega r'^2 n(r') \frac{m_H}{X} . dr' = \frac{\Omega}{3-\omega} n_0 r_0^{\omega} r^{3-\omega} \frac{m_H}{X} \quad (2)$$

where m_H/X is conversion factor from hydrogen number density to mass density, and X is the hydrogen mass fraction in the gas. We also define a characteristic mass density $\rho_0 \equiv n_0 m_H/X$.

3. Weaver solution (Weaver 1977)

For $\omega = 2$ and $\Omega = 4\pi$, Equation 7 becomes

$$r_{w,2}(t) = 13.9 \text{ pc} \left(\frac{L_w}{10^{36} \text{ erg/s}}\right)^{1/3} \left(\frac{n_0}{1000 \text{ cm}^{-3}}\right)^{-1/3} \left(\frac{t}{1 \text{ Myr}}\right), \quad (9)$$

which has a constant expansion velocity

$$v_{w,2} = 13.5 \text{ km/s} \left(\frac{L_w}{10^{36} \text{ erg/s}}\right)^{1/3} \left(\frac{n_0}{1000 \text{ cm}^{-3}}\right)^{-1/3} . \quad (10)$$

2

The dynamical equations governing the wind bubble's expansion are

$$E_b = \frac{3}{2} \frac{\Omega}{3} r_w^3 P_w, \quad (3)$$

$$\frac{d}{dt}\left(M(<r_w)\frac{dr_w}{dt}\right) = \Omega r_w^2 P_w, \quad (4)$$

and

$$\frac{dE_b}{dt} = L_w - \Omega r_w^2 P_w \frac{dr_w}{dt}, \quad (5)$$

where E_b is the thermal energy in the shocked gas inside the wind bubble and P_w is the pressure from the wind bubble acting on the inside of the shell. Equation 4 describes the conservation of momentum, and Equation 5 describes the conservation of energy. The first term on the right hand side of this latter equation, L_w, is the wind luminosity of the central source, i.e. the mechanical power of the material ejected by the star, assumed constant here for simplicity. The second right hand side term is the work done by the gas pressure P_w. The temperature and density of the wind bubble are not immediately important in deriving this solution. We give estimates for these quantities in Section 5.3.

Windで掃くシェルの時間進化

The dense, wind-swept shell is typically dense enough that the recombination time of the gas is short, and hence we assume photoionisation equilibrium, i.e. the photons emitted by the star in the solid angle of the shell are all absorbed by the shell. We can write the balance of photon emission and absorption as

$$\frac{\Omega}{4\pi} Q_{\rm H} = \int_{r_{\rm w}}^{r_{\rm i}} \Omega r^2 n_{\rm i}^2(r) \alpha_{\rm B} . dr \tag{11}$$

where $Q_{\rm H}$ is the ionising photon emission rate, $n_{\rm i}(r)$ is the hydrogen number density in the photoionised gas at a radius r and $\alpha_{\rm B}$ is the Baker & Menzel (1938) case B recombination rate of the gas for HII, which is 2 to 3×10^{-13} cm^3 s^{-1} at solar metallicity. The exact formula used to calculate $\alpha_{\rm B}$ depends on the temperature of the photoionised gas and is given in Appendix E2 of Rosdahl et al. (2013).

bubble. Draine (2011) gives the conditions for hydrostatic pressure balance, ionising photon balance and dust absorption optical depth respectively at radius r inside the photoionised shell as

$$n_{\rm i}\sigma_{\rm d}\frac{(L_{\rm n}e^{-\tau}+L_{\rm i}\phi)}{4\pi r^2 c} + \alpha_{\rm B} n_{\rm i}^2 \frac{\langle h\nu\rangle_{\rm i}}{c} - \frac{\rm d}{{\rm d}r}(2n_{\rm i}(r)k_{\rm B}T_{\rm i}) = 0, \tag{12}$$

$$\frac{{\rm d}\phi}{{\rm d}r} = -\frac{1}{Q_{\rm H}}\alpha_{\rm B} n_{\rm i}^2 4\pi r^2 - n_{\rm i}\sigma_{\rm d}\phi, \tag{13}$$

and

$$\frac{{\rm d}\tau}{{\rm d}r} = n_{\rm i}\sigma_{\rm d}, \tag{14}$$

We solve these equations beginning at $r_{\rm w}$, where the density $n_{\rm i}$ is set by the pressure balance with the wind bubble,

$$P_{\rm w} = P_{\rm i} \equiv \frac{m_{\rm H}}{X} n_{\rm i} c_{\rm i}^2 \tag{15}$$

(e.g. Dyson & Williams 1980), where $P_{\rm w}$ is given in Equation 5. We integrate for increasing r until ϕ reaches zero, i.e. all the ionising photons have been absorbed, which we define as the edge of the photoionised shell $r_{\rm i}$.

For each value of $r_{\rm w}$ we use, we calculate the mass of the photoionised shell

$$M_{\rm i} = \int_{r_{\rm w}}^{r_{\rm i}} \Omega r^2 n_{\rm i}(r) \frac{m_{\rm H}}{X} . dr, \tag{16}$$

and compare it to the total mass of gas swept up by the HII region out to $r_{\rm i}$, $M(<r_{\rm i})$ using Equation 2. If the value found for Equation 16 exceeds $M(<r_{\rm i})$, the solution breaks down because there is no more mass in the neutral shell to absorb the ionising photons. We refer to

- 電離で掃くシェルの時間進化
- M(rw)~M(ri)でシェルの中にionizeするガスが残っていないので、champagne flowが起こる

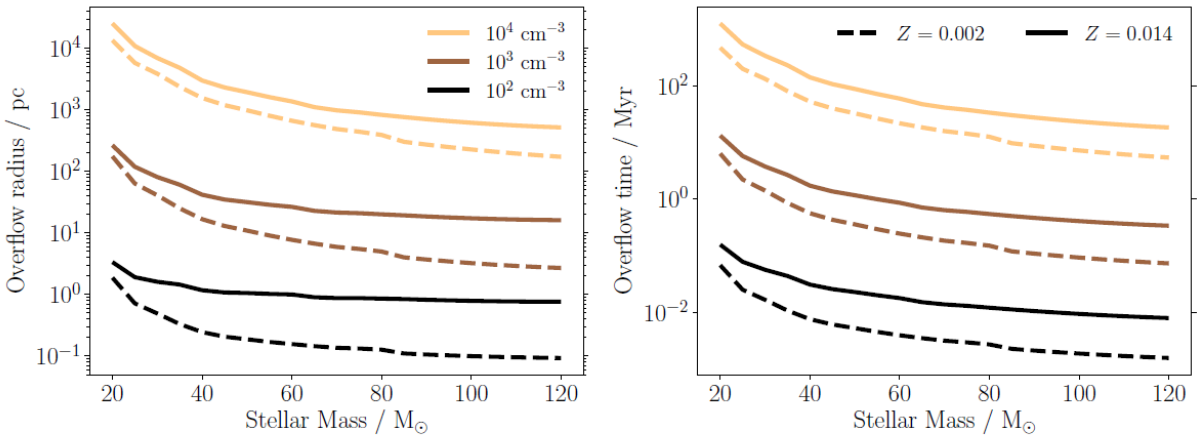

Figure 4. Point at which ionising photon overflow occurs as a function of initial stellar mass, with varying metallicity and characteristic background hydrogen number density n_0, where $n(r) = n_0(r\ /\ 1\ \mathrm{pc})^{-2}$. The left plot shows the outer radius of the ionised shell r_i at which overflow occurs, the right plot shows the time of overflow. The denser the environment, the denser the shell around the wind bubble and hence the longer it takes for ionising photons to overflow the shell. Due to weaker winds, overflow occurs sooner and at smaller radii at lower metallicity. Solid lines show results at Solar metallicity ($Z = 0.014$) and dashed lines show results at sub-Solar metallicity ($Z = 0.002$). Line colour shows characteristic cloud density n_0.

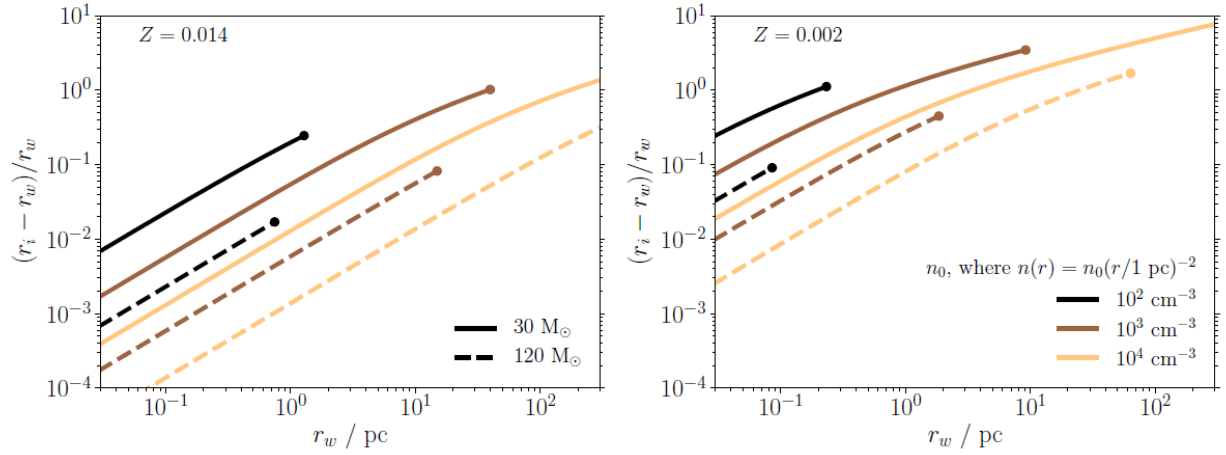

Figure 5. Relative thickness of the photoionised shell $r_\mathrm{i} - r_\mathrm{w}$ against the wind bubble radius r_w, plotted as a function of r_w with varying initial stellar mass and characteristic background hydrogen number density n_0, where $n(r) = n_0(r\ /\ 1\ \mathrm{pc})^{-2}$. The left plot shows results at $Z = 0.014$, and the right plot shows results at $Z = 0.002$. Dashed lines show results for a 120 M$_\odot$ star, solid lines show results for a 30 M$_\odot$ star. Line colour shows characteristic cloud density n_0. The relative thickness of the ionised shell is typically small until near the point of overflow, which is shown as a circle at the end of each line. We omit results after 250 pc since this is larger than most molecular clouds in our Galaxy and nearby galaxies. We also note that substructure in complex star-forming environments is likely to cause the power law density distribution to break down at smaller radii than this. In this scenario, photon breakout will be caused by 3D effects before the HII region reaches the overflow point.

オリオンの場合

Geometry		Shell velocity	Age	Overflow radius
r_i / pc	Ω	$\mathrm{d}r_\mathrm{i}/\mathrm{d}t$ / km/s	t / Myr	$r_{\mathrm{o},2}$ / pc
Stellar mass = 30 M$_\odot$				
2.0	4π	$9.6^{+4.8}_{-1.7}$	$0.215^{+0.042}_{-0.067}$	$44.4^{+40.5}_{-32.4}$
4.0	1π	$11.1^{+4.7}_{-1.7}$	$0.359^{+0.065}_{-0.103}$	$282.2^{+257.0}_{-205.9}$
Stellar mass = 35 M$_\odot$				
2.0	4π	$11.7^{+5.6}_{-2.0}$	$0.176^{+0.033}_{-0.053}$	$37.7^{+34.3}_{-27.5}$
4.0	1π	$13.7^{+5.7}_{-2.1}$	$0.290^{+0.052}_{-0.083}$	$239.2^{+217.8}_{-174.5}$

Table 1. Table showing the results of our model for the conditions in the Orion Nebula. We follow two stellar tracks, one at 30 M$_\odot$ and one at 35 M$_\odot$ in order to capture the uncertainty in the stellar mass measurement for θ^1 Ori C. We further adopt two models for the nebula structure, visualised in Figure 8. In the first model, the initial gas mass distribution and the stellar

Overflowが起こる半径

neutral gas. We can write a condition for such photon "overflow" as

$$\frac{\Omega}{3-\omega} n_0 r_0^{\omega} r_\mathrm{w}^{3-\omega} \frac{m_\mathrm{H}}{X} \leq \frac{\Omega}{3}\left(r_\mathrm{i}^3 - r_\mathrm{w}^3\right) n_\mathrm{i} \frac{m_\mathrm{H}}{X} \tag{24}$$

Making the same substitutions for n_i and t as in Section 4.1, we can produce an expression for the wind bubble radius at which overflow is possible, where

$$r_\mathrm{w}^{\frac{5-4\omega}{3}} \leq \frac{\Omega}{4\pi}\left(\frac{3-\omega}{2}\right)\left(\frac{11-\omega}{5-\omega}\right)\frac{Q_\mathrm{H} c_\mathrm{i}^2}{\alpha_\mathrm{B}}\left(\frac{m_\mathrm{H}}{X}\frac{A_\mathrm{w}^{1/2}(\omega,\Omega)}{L_\mathrm{w} n_0^2 r_0^{2\omega}}\right)^{2/3} \tag{25}$$

A wind-blown bubble in the Central Molecular Zone cloud G0.253+0.016

Jonathan D. Henshaw,[1⋆] Mark R. Krumholz,[1,2,3,4] Natalie O. Butterfield,[5] Jonathan Mackey,[6,7]
Adam Ginsburg,[8] Thomas J. Haworth,[9] Francisco Nogueras-Lara,[1] Ashley T. Barnes,[10] Steven N. Longmore,[11]
John Bally,[12] J. M. Diederik Kruijssen,[13] Elisabeth A. C. Mills,[14] Henrik Beuther,[1] Daniel L. Walker,[15]
Cara Battersby,[15] Alyssa Bulatek,[8] Thomas Henning,[1] Juergen Ott,[16,17] and Juan D. Soler,[1]

G0.253+0.016, commonly referred to as "the Brick" and located within the Central Molecular Zone, is one of the densest ($\approx 10^{3-4}\,\mathrm{cm^{-3}}$) molecular clouds in the Galaxy to lack signatures of widespread star formation. We set out to constrain the origins of an arc-shaped molecular line emission feature located within the cloud. We determine that the arc, centred on $\{l_0, b_0\} = \{0.^{\circ}248, 0.^{\circ}018\}$, has a radius of 1.3 pc and kinematics indicative of the presence of a shell expanding at $5.2^{+2.7}_{-1.9}\,\mathrm{km\,s^{-1}}$. Extended radio continuum emission fills the arc cavity and recombination line emission peaks at a similar velocity to the arc, implying that the molecular and ionised gas are physically related. The inferred Lyman continuum photon rate is $N_{\mathrm{LyC}} = 10^{46.0}$-$10^{47.9}\,\mathrm{photons\,s^{-1}}$, consistent with a star of spectral type B1-O8.5, corresponding to a mass of $\approx$ 12-20 $\mathrm{M_\odot}$. We explore two scenarios for the origin of the arc: i) a partial shell swept up by the wind of an interloper high-mass star; ii) a partial shell swept up by stellar feedback resulting from in-situ star formation. We favour the latter scenario, finding reasonable (factor of a few) agreement between its morphology, dynamics, and energetics and those predicted for an expanding bubble driven by the wind from a high-mass star. The immediate implication is that G0.253+0.016 may not be as quiescent as is commonly accepted. We speculate that the cloud may have produced a $\lesssim 10^3\,\mathrm{M_\odot}$ star cluster $\gtrsim 0.4$ Myr ago, and demonstrate that the high-extinction and stellar crowding observed towards G0.253+0.016 may help to obscure such a star cluster from detection.

A wind-blown bubble in the Central Molecular Zone cloud G0.253+0.016

- G0.253+0.016 (the Brick): Central Molecular Zoneにある星形成していないと思われていた分子雲
- ALMA Early Science Cycle 0 Band 3 (Rathborne+2014, 2015)のデータ
- ScoursePyとACORNSで解析→HNCO

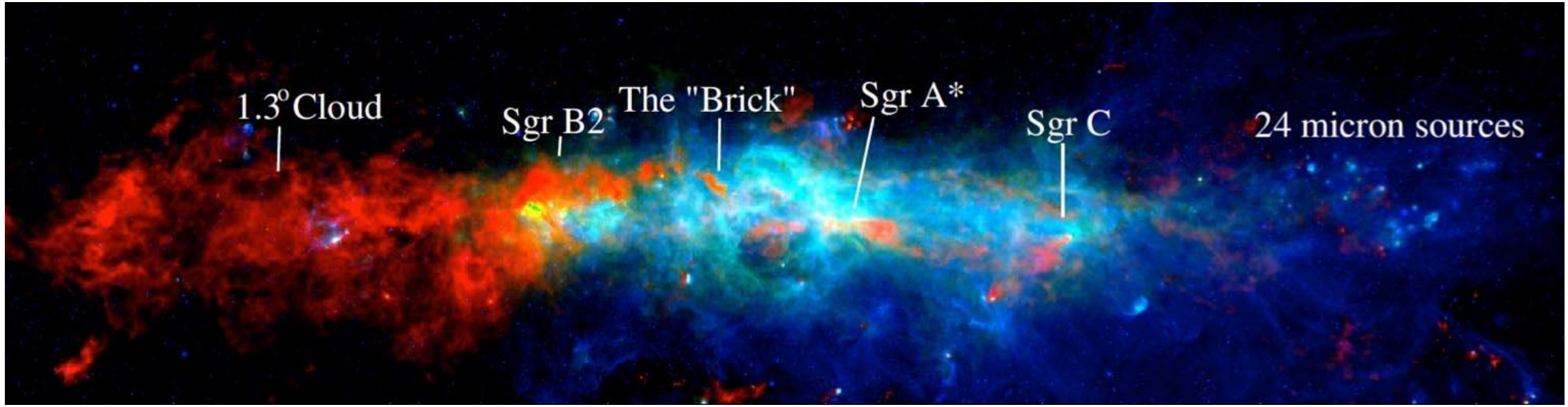

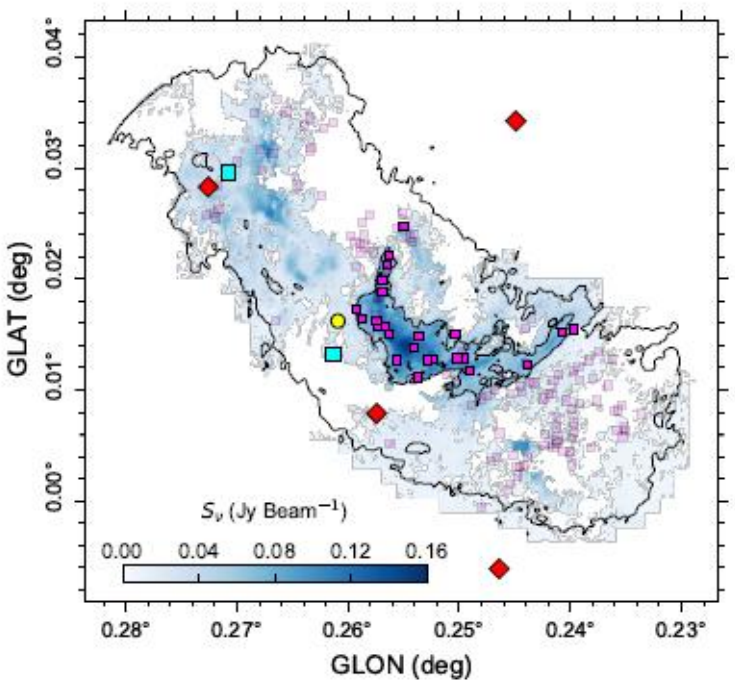

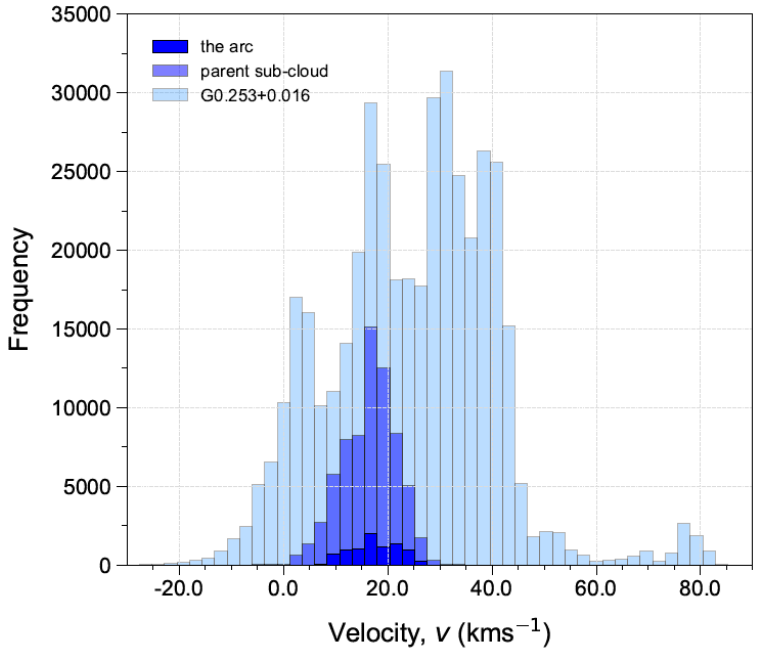

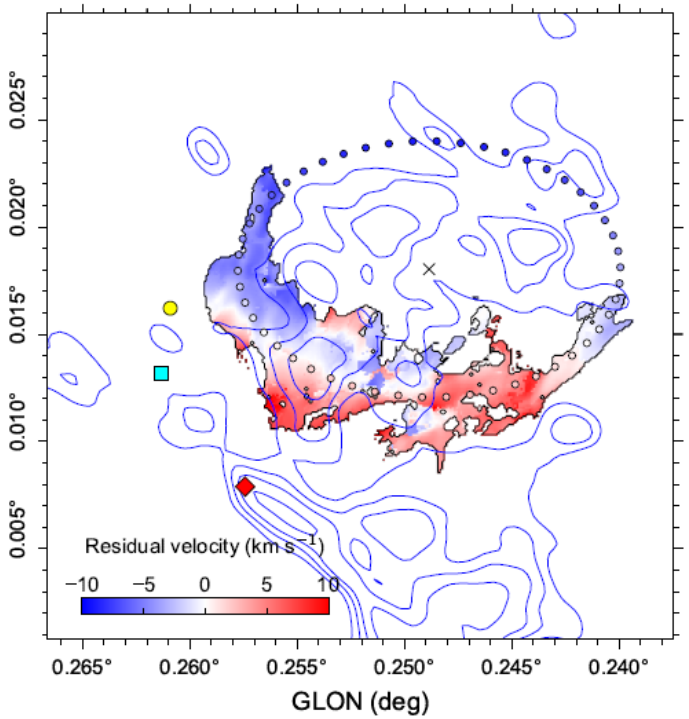

HNCOの強度マップ
黄丸、シアン四角：水メーザー
マゼンタ四角：CH3OHメーザー
赤：HII領域

バルク速度を引いた後のアークの速度
→expanding shell

- アークの広がる速度：$5.2^{+2.7}_{-1.9}$ km/s
- アークの質量の見積もり2700Msun
- アークを作れるような電離源：NLyC=$10^{46\text{-}47.9}$ photons/s →12－20Msunの星
- Salpeter IMFを仮定して、数百Msunの星団がある？
- アークを作った星は、そこで生まれたのでは？